Chemical Science

ROYAL SOCIETY OF CHEMISTRY

EDGE ARTICLE

View Article Online
View Journal | View Issue

Cite this: *Chem. Sci.*, 2025, **16**, 288

All publication charges for this article have been paid for by the Royal Society of Chemistry

Facile construction of polyoxometalate-polymer hybrid nanoparticles with pH/redox dual-responsiveness†

Yanting Gao,[ab] Fan Yang,[a] Yufu Wang,[a] Angus P. R. Johnston,[c] Rebekah N. Duffin,[b] Philip C. Andrews,[b] Chris Ritchie *[b] and Georgina K. Such *[a]

Received 11th June 2024
Accepted 6th November 2024

DOI: 10.1039/d4sc03814b

rsc.li/chemical-science

Responsive nanomaterials have emerged as promising candidates for advanced drug delivery systems (DDSs), offering the potential to precisely target disease sites and enhance treatment efficacy. To fulfil their potential, such materials need to be engineered to respond to specific variations in biological conditions. In this work, we present a series of pH/redox dual-responsive hybrid nanoparticles featuring an amphiphilic shell polymer and a pH-responsive core polymer. These nanoparticles incorporate a polyoxometalate (POM), specifically the cobalt(III)-substituted borotungstate ($[B^{III}W_{11}O_{39}Co^{III}]^{6-}$), loaded through coordination chemistry between the encapsulated Co^{III} ions of the POM and pyridyl functional groups on the core polymer. The resulting hybrid nanoparticles show potential for controlled release with excellent stability at physiological pH, and efficient particle disassembly in response to the combination of pH and redox stimuli. Disassembly is proposed to occur following a two step mechanism. Structural rearrangement of the nanoparticle occurs on acidification followed by destabilization of the coordination bond between the polyanion and the pyridyl functionality in the core polymer following reduction. In this system, the POM acts in a novel role as a redox active structural cross-linker. These hybrid dual-responsive nanoparticles, featuring superior colloidal stability under extracellular conditions and controllable disintegration in response to the dual stimuli of acidic pH and redox conditions, provide a novel platform for the controlled intracellular release of therapeutics.

Introduction

Nanoparticle-based drug delivery systems (DDSs) are considered one of the most viable platforms for improving the therapeutic efficacy of drugs by protecting therapeutic cargo, and facilitating controlled delivery at specific treatment sites.[1–4] Many types of nanoparticles have been investigated to deliver therapeutics, including liposomes, inorganic particles, and polymeric particles.[5–8] Among the array of DDSs, polymeric nanoparticles stand out due to their tuneable composition and the vast array of chemical functionalities they can incorporate. These characteristics enable the realisation of sophisticated designs and provide substantial potential to integrate stimuli-responsive functionalities, thereby allowing these systems to precisely control cargo release.

Stimuli-responsive DDSs have been designed using a range of endogenous stimuli, such as redox potential, pH, or enzyme concentration, with on-demand release of therapeutics being achieved, thereby minimizing side effects.[9–13] Specifically, pH and redox potential triggers are particularly interesting due to the inherent pH and redox variations across different biological environments.[14–16] Following intravenous injection, polymeric nanoparticles can be internalized by cells through endocytosis with accumulation in the late endosome and lysosome where the pH is 2–3 units lower (pH 4.7–5.5) than that of the extracellular media (pH 7.4).[17] Furthermore, the target site for the majority of therapeutics is the nucleus or cytosolic region of the cell. The cytosol is considerably more reducing compared to the extracellular plasma, with glutathione (GSH) concentration spanning several orders of magnitude (2 μM–10 mM).[18] Consequently, a common design strategy for smart DDSs is to use variation in pH or redox stimuli to facilitate nanoparticle response.

To design pH responsive DDSs a well-reported approach is based on use of tertiary amine monomers. These monomers can

[a]School of Chemistry, The University of Melbourne, Parkville, 3010, Victoria, Australia. E-mail: gsuch@unimelb.edu.au

[b]School of Chemistry, Monash University, Clayton, 3800, Victoria, Australia. E-mail: chris.ritchie@monash.edu

[c]Monash Institute of Pharmaceutical Sciences, Monash University, Parkville, Victoria 3052, Australia

† Electronic supplementary information (ESI) available: Detailed experimental procedure for the synthesis of core/shell polymers, nanoparticle formation, cell viability test, and supporting figures including ^{1}H NMR spectra, SEC, UV-vis spectra, FT-IR spectrum, NTA and cytotoxicity. See DOI: https://doi.org/10.1039/d4sc03814b

be incorporated into the hydrophobic block of an amphiphilic polymer with exceptional compositional control, achieved through controlled polymerization techniques such as atom transfer radical polymerization (ATRP) and reversible addition-fragmentation chain transfer (RAFT). When the ionizable groups are protonated they display a notable increase in hydrophilicity, leading to a transition of this block from hydrophobic to hydrophilic and thus particle disassembly.[19,20] Two such charge shifting polymers, poly(2-diethylamino ethyl methacrylate) (PDEAEMA) and poly(2-diisopropylamino ethyl methacrylate) (PDPAEMA), have been shown to form pH-responsive nanoparticles where the ratio of DEAEMA and DPAEMA affords control over the disassembly pH.[21,22]

Previously, we demonstrated that engineering the nanoparticle disassembly pH could significantly impact biological interactions, including increasing endosomal escape efficiency up to fivefold.[23] However, designing stimuli-responsive delivery systems based solely on pH responsive capabilities can limit the stability in the blood-stream, leading to premature release of drugs from self-assembled nanoparticles. To improve the stability of such systems two feasible strategies have been extensively studied: cleavable linkages between drug molecules and the polymer matrix, and crosslinking of the core or shell in self-assembled polymeric nanoparticles.[24–26] Both approaches have been shown to improve the stability of encapsulated drugs at physiological pH while enabling more controlled release at the intended therapeutic sites. An especially promising method involves crosslinking through disulfide bonds, which are susceptible to cleavage in the intracellular environment due to the presence of the strongly reducing environment in the cytosol.[27] This is an attractive approach to construct core-crosslinked nanoparticles with controlled intracellular drug release.[28] There is a significant body of research on the use of disulfide bonds as redox-responsive crosslinkers in nanoparticle-based drug delivery systems. Black phosphorus and MnO_2 have also been employed to form inorganic nanosheets with redox responsiveness, functioning as nanoprobes or bioactive anti-cancer agents.[29,30] However, to the best of our knowledge, there is no literature demonstrating the use of an embedded inorganic cargo within polymeric nanoparticles to impart redox-responsive capabilities.

Polyoxometalates (POMs) are molecular anions characterised by their composition of metal ions in high oxidation states and oxide ligands, exhibiting an exceptional range of structural diversity, compositional variety, redox potential, and charge distribution.[31,32] This unique set of properties underscores their significance and versatility in various chemical applications.[33,34] The potential of POMs as antiviral, anticancer, and antibacterial agents has been the subject of extensive research over many years, with a recent resurgence,[35–39] revealing promising therapeutic activities. For example, Yamase and co-workers evaluated the anticancer activities of $[NH_3\text{-}Pr^i]_6[Mo_7O_{24}]$ (PM-8), demonstrating its high efficiency in suppressing tumour growth both *in vitro* and *in vivo*.[40] In their following works, they proposed a mechanism for the anticancer activity of PM-8 involving its reduction and re-oxidation, which led to the killing of tumour cells.[41] However, purely inorganic POMs often suffer from high toxicity and non-specific interactions with biomolecules, severely impeding their clinical applications. Various strategies have been employed to reduce the toxicity and enhance targeting capabilities, such as direct surface modification or integration with polymeric materials to form nanoparticles. The introduction of organic moieties into the POM framework can alter its surface chemistry, charge, polarity, and redox properties, resulting in a new compound with reduced toxicity and increased cell penetration ability.[42] Encapsulation of POMs into nanoparticles is another strategy to enhance their stability and solubility, reduce cytotoxicity, and extend the circulation time by preventing undesired interactions during the delivery process. Recently, we reported the design of pH-responsive core–shell nanoparticles that successfully incorporated cobalt(III)-substituted borotungstate cargo, $[B^{III}W_{11}O_{39}Co^{III}]^{6-}$ *via* coordination chemistry. This specific Keggin polyanion was selected for its low oxidation power, exceptional stability in aqueous media, and its capacity to form kinetically inert coordination bonds between the encapsulated Co^{III} ions and the pyridyl functional groups on the core polymer of the core–shell particles.[43] In that initial study, the incorporation of POMs into these charge-shifting nanoparticles significantly altered their pH responsiveness, leading to a notable structural rearrangement in response to acidification, rather than the complete disassembly observed in POM-free control nanoparticles.

Herein, we demonstrate the potential of POM-polymer hybrid nanoparticles as dual pH/redox responsive systems. These particles were assembled using amphiphilic shell polymers (**SP**), poly(ethylene glycol methacrylate)-*b*-poly(2-(diethylamino)ethyl methacrylate) P(PEGMA-*b*-DEAEMA), charge shifting core polymers (**CP**), poly(2-(diethylamino) ethyl methacrylate-*r*-2-(diisopropylamino) ethyl methacrylate-*r*-4-(pyridyl) methyl methacrylate) P(DEAEMA-*r*-DPAEMA-*r*-PyMMA), and the redox active Keggin polyanion $[B^{III}W_{11}O_{39}Co^{III}]^{6-}$ (Fig. 1). The pyridyl functionality in **CP** provided an anchor point for coordination with POMs. By varying the PyMMA content from 1 mol% to 5 mol% (designated as 1%Py@CP, 3.5%Py@CP, 5% Py@CP), we synthesized a library of **CP**s with different POM contents. The resulting hybrid nanoparticles, featuring a PEG shell and a POM-loaded core, were prepared through self-assembling with amphiphilic **SP**. These hybrid assemblies exhibited superior colloidal stability at physiological pH, yet showed tuneable stability upon acidification, determined by the POM loading content with particles containing higher amounts showing good stability with pH. Interestingly, the addition of 5 mM dithiothreitol (DTT) showed little impact on particle stability at pH 7.4 but when it was combined with a decrease in pH efficient disassembly of the particles was observed. This suggested the synergistic behaviour of pH and redox potential on particle behaviour. This can be attributed to the proton coupled electron transfer (PCET) observed for the Co(III) ion in Keggin anion. This reduction process is also dependant on pH due to the structural arrangement of nanoparticles in acidic conditions, which induces a significant hydrophilic transition within the nanoparticles, thereby facilitating the redox reaction. The reduction of cobalt from Co^{III} (d^6, ls) to Co^{II} (d^7, hs),

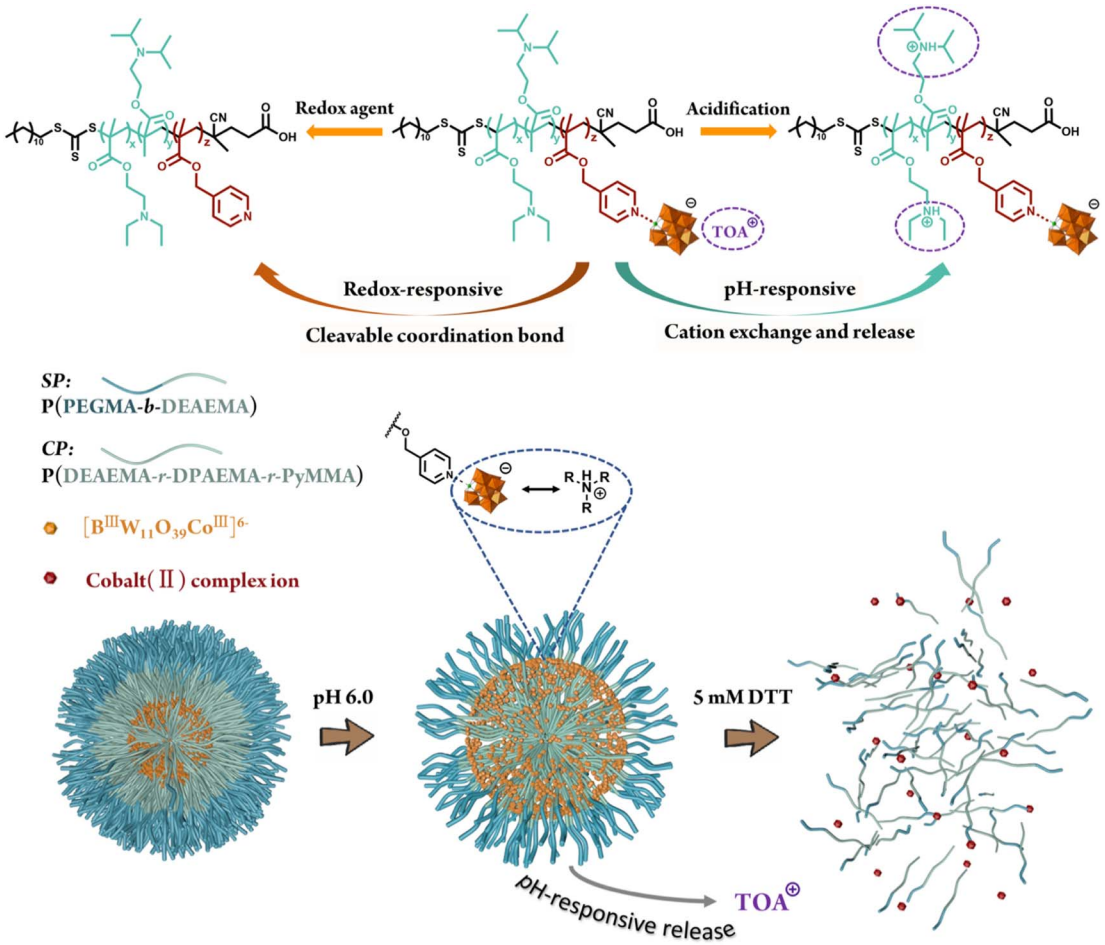

Fig. 1 Schematic illustration of the pH/redox dual responsive hybrid nanoparticles comprising the amphiphilic shell polymer, P(PEGMA-*b*-DEAEMA) (**SP**), charge-shifting core polymer, P(DEAEMA-*r*-DPAEMA-*r*-PyMMA) (**CP**), and cobalt(III)-substituted borotungstate, $[B^{III}W_{11}O_{39}Co^{III}]^{6-}$. These nanoparticles exhibited structural changes in response to acidification accompanied by cation exchange to release tetra-octyl ammonium (TOA), the charge-balancing cations for POM, and subsequently underwent disassembly upon treatment with a reducing agent dithiothreitol (DTT).

facilitated the destabilization of the POM-polymer coordination bonds leading to particle disassembly. Overall, these pH-sensitive nanoparticles, incorporating redox-responsive POM cross-linkers, exhibited promising colloidal stability under extracellular conditions and synergistic disassembly behaviour in response to the dual stimuli of acidic pH and redox conditions. This innovative platform therefore displays dual response properties commensurate with that desired for the intracellular controlled release of therapeutics.

Results and discussion

Polymerization and characterization

In this study, the amphiphilic P(PEGMA-*b*-DEAEMA) (**SP**), and a series of charge shifting P(DEAEMA-*r*-DPAEMA-*r*-PyMMA) with varying compositions (**CP**s), were synthesized *via* RAFT polymerization (Scheme 1). The charge-shifting monomers, DEAEMA and DPAEMA, were used to yield pH-responsive nanoparticles, and their molar ratio was maintained consistently as 1 : 1 to ensure a similar pK_a value across all **CP**s. A small amount of the third monomer (1 mol%, 3.5 mol% and 5 mol%), PyMMA, was incorporated into the **CP** backbone to facilitate the coordination of the polymer with the Co^{III} incorporated POM during post-polymerization modification (See ESI† for methodology). The polymers were characterized by ^{1}H Nuclear Magnetic Resonance (NMR) and Size Exclusion Chromatography (SEC). The number average molecular weight (M_n) of **SP** was 25.7 kDa based on ^{1}H NMR spectra. For **CP**s with different PyMMA ratios (designated as 1%Py@CP, 3.5%Py@CP, and 5%Py@CP), the Mn values were 28.7 kDa, 29.2 kDa, and 29.5 kDa, respectively. SEC analysis yielded dispersities of 1.23 for **SP**, and 1.25, 1.29, and 1.25 for 1%Py@CP, 3.5%Py@CP, and 5%Py@CP, respectively (Table S1 and Fig. S1–S9†).

Coordination bond formation and DTT-induced cleavage

The polyoxometalate used in this study $(TOA)_{6-x}H_x[B^{III}W_{11}{}^{VI}O_{39}Co^{III}]$ was prepared as described in our previous study.[44] The coordination of the POM with each **CP** was monitored and quantified using ^{1}H NMR spectra. To minimise the association

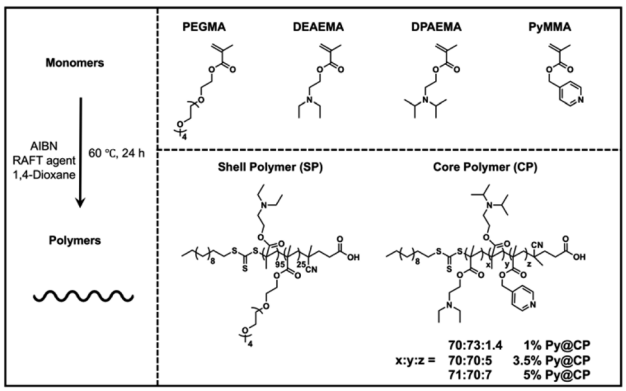

Scheme 1 RAFT polymerization reaction scheme and structures of four different monomers, amphiphilic **SP**, P(PEGMA$_{25}$-*b*-DEAEMA$_{95}$), and three charge-shifting **CP**s, P(DEAEMA$_{70}$-*r*-DPAEMA$_{73}$-*r*-PyMMA$_{1.4}$), P(DEAEMA$_{70}$-*r*-DPAEMA$_{70}$-*r*-PyMMA$_{5}$), and P(DEAEMA$_{71}$-*r*-DPAEMA$_{73}$-*r*-PyMMA$_{7}$). Azobisisobutyronitrile (AIBN) was utilized to initiate the polymerization.

of POMs with the **CP**s through interactions other than coordination bonds, a sub stoichiometric amount of POM was added to each respective **CP**. This was achieved by adding TOA salts of POM (0.22 μmol, 0.54 μmol, and 1.07 μmol) to a 0.17 mM acetone stock solution (900 μL) of each **CP**, resulting in a loading of approx. 80%.

The cleavage of coordination bonds under mild reductive conditions was investigated by introducing DTT at a concentration of 5 mM into the previously described **POM-CP** stock solutions. DTT is a thiol containing GSH surrogate frequently used to mimic the reducing intracellular environment encountered during drug delivery experiments.[45] The ^{1}H NMR spectra, highlighted in Fig. 2 for 5% Py@CP, clearly showed peak shifts following the addition of POM, with recovery of the initial spectra following incubation of the POM-polymer hybrid with DTT. The ^{1}H resonance peaks of H_A and H_B shifted downfield ($\Delta\delta \approx 0.07$ ppm) and upfield ($\Delta\delta \approx -0.09$ ppm), respectively, on complexation of the POM, indicating successful coordination.[44] Recovery of the initial spectra occurred on addition of 100 μL DTT solution (50 mM) to the 900 μL **POM-CP** stock solution. A 12 hours incubation of the samples at room temperature was sufficient to achieve full conversion (Fig. 2, S10 and S11†). Meanwhile, the apparent colour of the solution changed from green to maroon, supporting the proposed change in cobalt oxidation state on reaction with DTT (Fig. S12†).[46] Collectively, these observations indicate that the coordination bond between $[B^{III}W_{11}O_{39}Co^{III}]^{6-}$ and pyridyl functionality can be easily formed *in situ*, and then rapidly destabilized due to the presence of DTT at low concentrations (5 mM). More importantly, the entire process can be efficiently tracked and quantified using ^{1}H NMR spectra.

Monitoring the evolution of the ^{1}H signature of oxidized DTT in this mixture is challenging due to its overlap with the broad, intense polymer peaks, however, the reaction of POM with DTT in the absence of any polymers as a control experiment has provided valuable information. The emergence of the characteristic ^{1}H resonance corresponding to oxidized DTT, following the addition of 0.5 mol equiv. of TOA salts of POM, confirmed the redox reaction between this mild reducing agent and cobalt(III)-substituted borotungstate (Fig. S13†). UV-vis spectroscopy and Fourier transform infrared (FT-IR) spectroscopy have been utilized to characterize the resulting inorganic product (Fig. S14 and S15†), however, we have been unsuccessful thus far in isolating a crystalline product suitable for structure elucidation using single crystal X-ray diffraction.

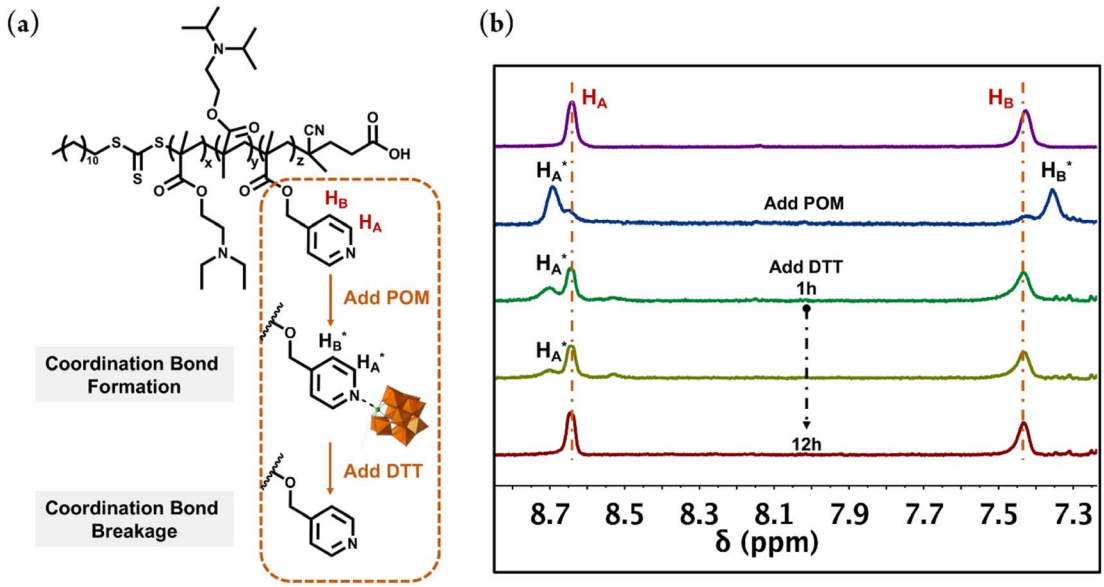

Fig. 2 The formation and breakage of coordination bonds monitored by proton NMR spectra. (a) Schematic representation of the random charge-shifting core polymer with coordinated POMs and the DTT-induced bond cleavage. (b) ^{1}H NMR spectra of 5%Py@CP in acetone-d_6, showing the change in the chemical shift of the pyridyl alpha-(H_A) and beta-protons (H_B) on coordination of POMs. * denotes coordination.

Assembly and characterisation of hybrid nanoparticles

The hybrid dual-responsive nanoparticles were formed by the nanoprecipitation technique with 1 : 1 (w/w) ratio of **SP** and each **CP**. **SP** (1.5 mg, 0.06 μmol) was added to a stock solution of **POM-CP** (300 μL, 0.05 μmol) in acetone and mixed thoroughly. This solution was then added dropwise into 3 mL phosphate-buffered saline (PBS, pH 8.0). Prior to characterisation, nanoparticles with different POM contents were purified *via* dialysis (24 h, MWCO 100 kDa) and size exclusion filtration (0.45 μM, PES) to yield 1%POM@NPs, 3.5%POM@NPs and 5% POM@NPs. DLS data demonstrated that 3.5%POM@NPs and 5%POM@NPs had diameters ranging between 180 and 220 nm at pH 8.0, while 1%POM@NPs displayed slightly smaller average diameters, falling between 130 and 170 nm at the same pH (Fig. 3a).

For the simultaneous quantification of nanoparticle size and concentration, nanoparticle tracking analysis (NTA) was applied. NTA yielded average sizes of 110, 145, and 160 nm for 1%POM@NPs, 3.5%POM@NPs and 5%POM@NPs, respectively. Furthermore, all hybrid nanoparticles exhibited an average concentration of approximately 1.7×10^{11} particles per mL as shown in Fig. 3b. Representative cryogenic transmission electron microscopy (Cryo-EM) images showed that these assemblies had a regular spherical structure at physiological pH, aligning with our previous report.[21] The POMs were predominantly encapsulated within the hydrophobic core of the nanoparticles. The lack of contrast between the hydration shell and the carbon grid, combined with the enhanced contrast of the POM-containing core, hampered visualisation of the hydrophilic shell region, resulting in observed sizes smaller than the hydrodynamic diameters indicated by DLS. Furthermore, the presence of tungsten markedly enhanced contrast, leading to images of hybrid nanoparticles captured *via* Cryo-EM to appear darker with increased POM loading as shown in Fig. 3c–e and S16–S19.† The small, irregular particles in Cryo-EM images are ice crystals formed during sample preparation.

pH/redox dual-responsiveness of hybrid nanoparticles

To study the pH responsiveness of POM-polymer nanoparticles, DLS measurements were recorded across a pH range of 8.0 to 6.0 at 37 °C, simulating the pH decrease observed during endocytosis. The POM free control particles, designated as 1% Py@NPs, 3.5%Py@NPs, and 5%Py@NPs, disassembled at around pH 6.4 regardless of the pyridyl ratio (Fig. S20†). The disassembly point is determined by low light scattering intensities and loss of a readable polydispersity index (PDI), which arise from protonation of the tertiary amines, leading to increased hydrophilicity, electrostatic repulsion, and ultimately nanoparticle disassembly.

Conversely, incorporation of POM into the **CP** disrupted the disassembly of the particles. These hybrid nanoparticles displayed sizes and stability comparable to those of the control groups within the pH range of 7.2–8.0. An unstable transition stage for 5%POM@NPs was noted from pH 7.0 to 6.6, a phenomenon previously reported and attributed to significant structural rearrangement resulting from cation exchange between TOA and protonated amine groups. In the current study, reduced fluctuations in particle size and PDI were observed by lowering the POM content to 3.5% and 1%. Both 3.5%POM@NPs and 1%POM@NPs maintained stable

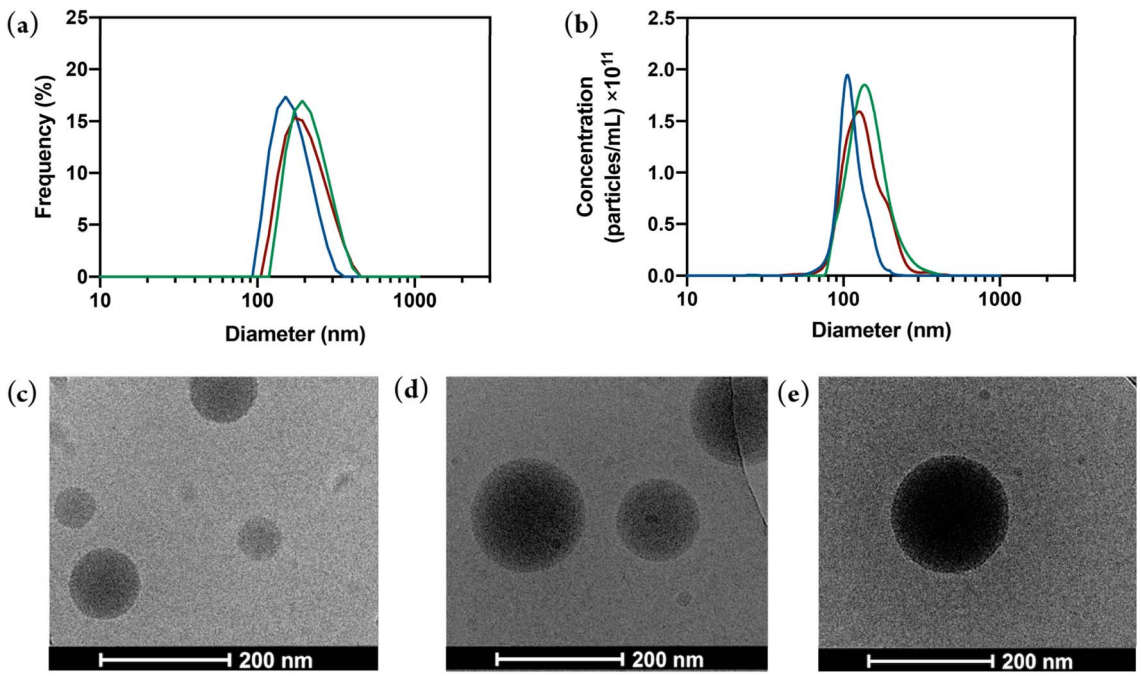

Fig. 3 Size distributions and morphology of the hybrid nanoparticles. (a) Intensity size distributions and (b) concentration size distributions of hybrid nanoparticles. 1%POM@NPs, 3.5%POM@NPs and 5%POM@NPs are shown in blue, red and green, respectively. Cryo-EM images of (c) 1% POM@NPs, (d) 3.5%POM@NPs, and (e) 5%POM@NPs. (Scale bar = 200 nm).

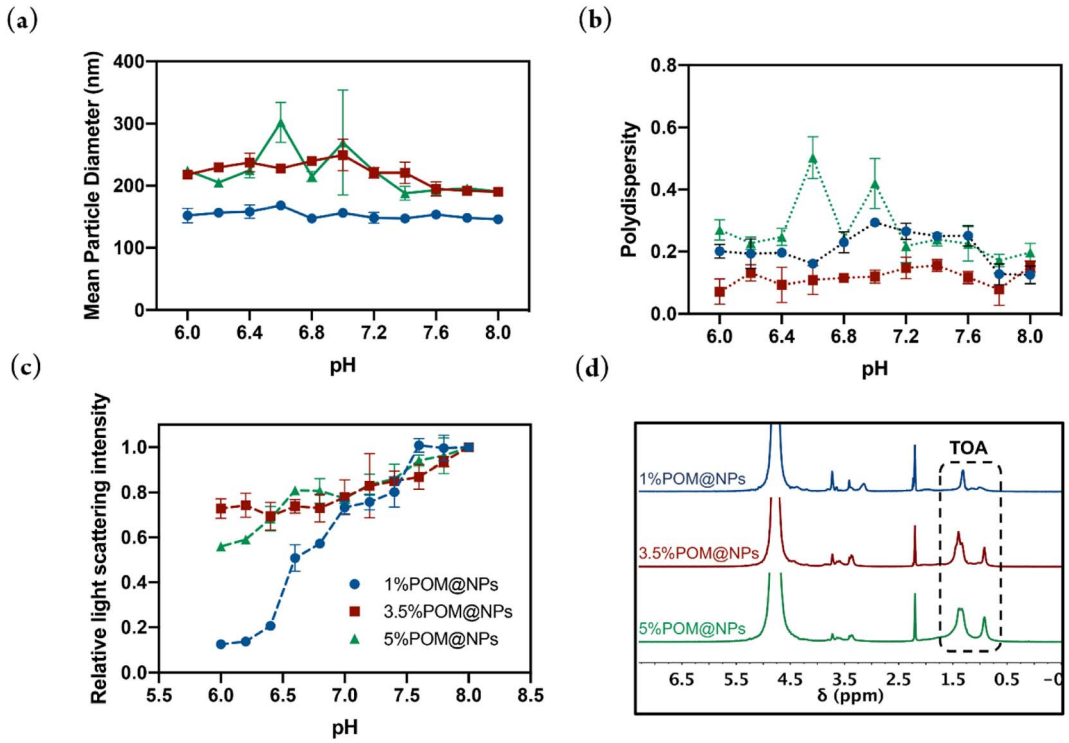

Fig. 4 The pH-responsiveness of hybrid nanoparticles. (a) Mean particle diameter, (b) polydispersity, and (c) relative light scattering intensity of 1%POM@NPs (blue), 3.5%POM@NPs (red) and 1%POM@NPs (green). (d) ^{1}H NMRs of hybrid nanoparticles in pH 6.0 PBS prepared using D_2O. Release of tetra-octyl ammonium (TOA) cations from within the nanoparticle core is observed. Error bars represent the standard deviation of the mean, calculated from three independent replicates ($n = 3$).

diameters and PDI values throughout the acidification process (Fig. 4a and b). The persistence of hybrid nanoparticles at pH 6.0 can be directly linked to the enhanced inter- and intra-polymer hydrogen bonding with the polyanion surface, alongside stronger point charge interactions, positioning POMs as effective cross-linking agents within this system. Therefore, it is reasonable to predict that the stability of nanoparticles under acidic conditions is predominantly governed by the POM concentration. The parameter of light scattering intensity was utilised to indirectly demonstrate changes in nanoparticle concentrations. As shown in Fig. 4c, the light scattering intensity of 1%POM@NPs dramatically declined with the decrease in pH value, retaining less than 10% at pH 6.0. This indicates that the majority of 1%POM@NPs disassembled during acidification. In contrast, the scattering intensities of 3.5%POM@NPs and 5%POM@NPs only showed a modest decrease in response to acidification, decreasing to approximately 75% and 60% at pH 6.0, respectively.

It is also worth mentioning that proton resonances associated with the TOA cations were absent at physiological pH (Fig. S21†), attributable to the isolation of the nanoparticle's hydrophobic region from the bulk solution, leading to significantly shorter spin–spin relaxation times (T_2) and the loss of signals in NMR spectra.[47] The sudden appearance of prominent signals of TOA (δ (ppm) 1.39, 1.33, and 0.92) at pH 6.0 can be explained by the partial disintegration of the nanoparticles, and more likely the release of the cations from the nanoparticles facilitated by cation exchange (Fig. 4d).

Both NTA and DLS were employed to further investigate the redox-induced disassembly of these hybrid materials. Unlike DLS, the intensity is dependent on the size, temperature and concentration of analytes, NTA provides a count-based concentration using low sample volumes, making it an ideal tool for directly monitoring the destabilisation process of particles. At physiological pH, all hybrid nanoparticles maintained nearly 100% particle concentrations with consistent mean diameters and PDI after 5 hours of incubation, regardless of the POM content and the presence or absence of DTT (Fig. 5a, b, and S22†). This observation underscored their exceptional colloidal stability, indicating the potential for such hybrid materials in therapeutic delivery. Given that pH 7.4 is higher than the pK_a of charge-shifting moieties PDEAEMA and PDPAEMA, the dense and hydrophobic nature of the particle core region restricted the free diffusion of DTT molecules, accounting for the observed stability under reducing conditions, also in agreement with results from the NMR experiment (Fig. S21†).

Next, the responsiveness of these systems was investigated with the combination of a decrease in pH and 5 mM DTT. At pH 6.0, the particle concentration of 1%POM@NP, as determined by NTA, experienced a drastic reduction by two orders of magnitude compared to its concentration at pH 7.4 before further incubation or the addition of DTT. This decrease in

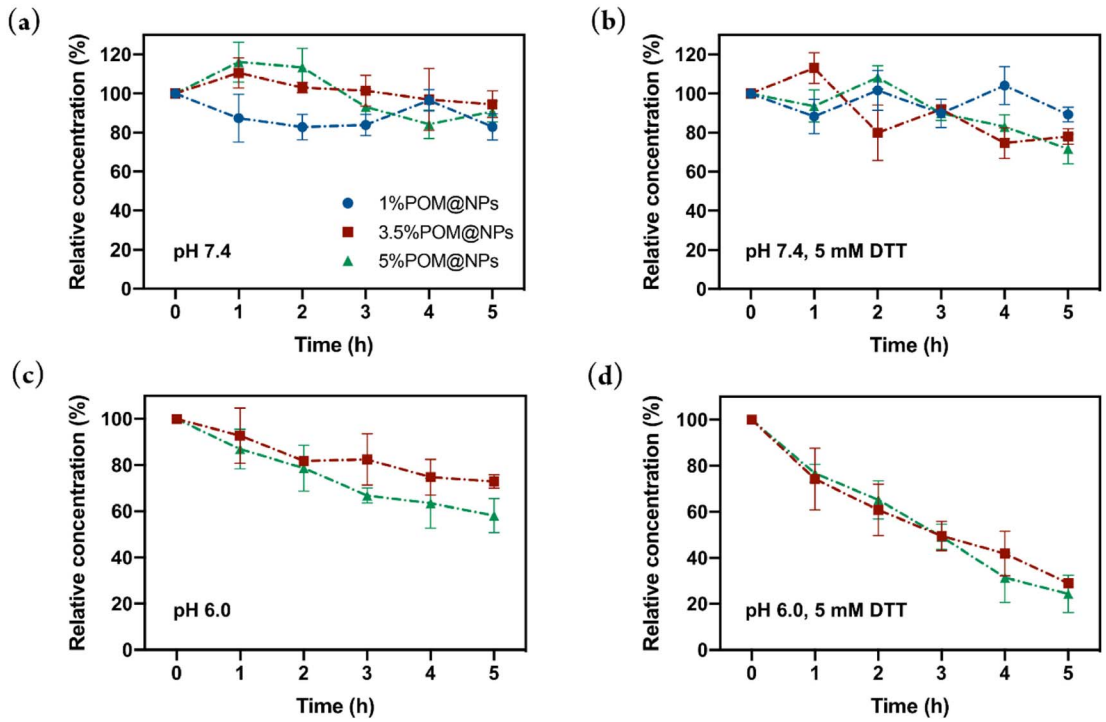

Fig. 5 pH and redox dual-induced changes in the particle concentration. The relative concentration of 1%POM@NPs (blue), 3.5%POM@NPs (red) and 1%POM@NPs (green) at pH value (a) 7.4, (b) 7.4 with addition of DTT, (c) 6.0, and (d) 6.0 with addition of DTT. Error bars represent the standard deviation of the mean, calculated from three independent replicates ($n = 3$).

concentration was accompanied by an increase in size distribution. (Fig. S23†). In contrast, 3.5%POM@NPs and 5% POM@NPs exhibited a gradual decline in nanoparticle concentration with decrease in pH, showing a reduction of approximately 30% after 5 hours of incubation (Fig. 5c). In contrast, a more notable decrease in particle concentration was observed when the two stimuli were combined for both 3.5% POM@NPs and 5%POM@NPs, with reduction of 70% and 80% respectively, after incubating these particles for 5 h at pH 6.0 in the presence of 5 mM DTT. This suggested the potential of these nanocarriers for targeted release in response to a combination of pH and redox variation (Fig. 5d). The loss of particles can be explained by the reduction of Co(III) and the subsequent cleavage of coordination bonds as discussed above, leading to diminished interaction between the polymers and polyanions, and the ultimate particle disassembly. Interestingly, the 3.5% POM@NPs demonstrated the most pronounced synergistic disassembly effect among the three hybrid nanoparticles examined. The acidification had the least influence on its nanoparticle concentration. However, the disintegration rate and ratio under dual stimuli conditions were comparable to those observed for the 5%POM@NPs.

Collectively, these observations demonstrated three principal characteristics of these dual-responsive hybrid systems. Firstly, they exhibit exceptional stability at physiological pH, both in the presence and absence of a reducing agent, maintaining consistent particle sizes and PDI. Secondly, the systems undergo notable structural rearrangement in response to acidification, with the amount of cross-linker—POMs, in this instance—demonstrating the capability to modulate their stability within mildly acidic environments. Thirdly, the introduction of a mild reducing condition (5 mM DTT) at pH 6.0, can disrupt the system within a short timeframe. Consequently, these attributes highlight their significant potential as novel DDSs, characterised by superior colloidal stability under extracellular conditions and rapid dissociation in response to the dual stimuli of acidic pH and mild reducing conditions.

In vitro cytotoxicity

After confirming the pH/redox responsive behaviour of hybrid nanoparticles, *in vitro* cytotoxicity of both POM-containing nanoparticles, 1%POM@NPs, 3.5%POM@NPs and 5% POM@NPs, and POM free control nanoparticles, 1%Py@NPs, 3.5%Py@NPs and 5%Py@NPs, were evaluated using Alamar Blue assay. All control nanoparticles were nontoxic (>90% viability) up to a particle concentration of 0.5×10^9 particles per mL, suggesting the POM-free materials possessed excellent biocompatibility with human embryonic kidney cells [HEK-293] (ATCC CRL-1573) within this concentration range. The half-maximal inhibitory concentration (IC_{50}) values of these particles were determined to be 3.7×10^9 particles per mL (Fig. 6a). Compared to the control groups, all hybrid nanoparticles exhibited increased toxicity. Notably, while 1%POM@NPs maintained a similar non-toxic concentration range as the control, they demonstrated a significantly lower IC_{50} value (0.8×10^9 particles per mL) in comparison to 1%Py@NPs. Both 3.5%POM@NPs and 5%POM@NPs demonstrated marked

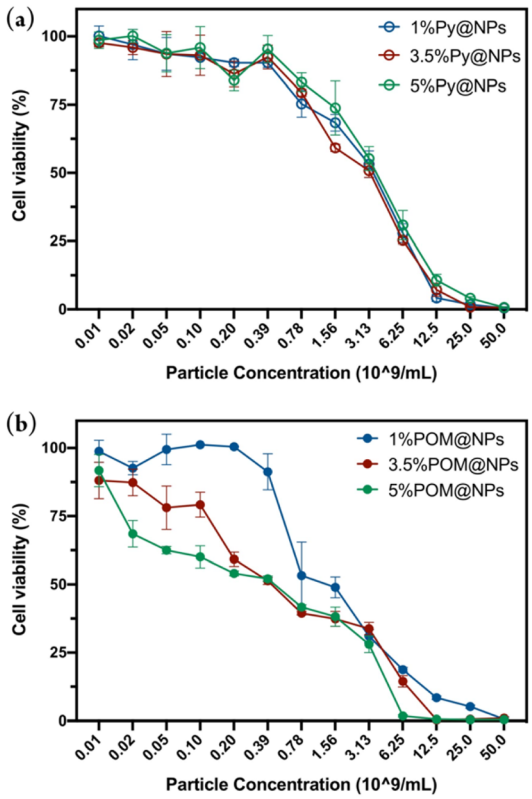

Fig. 6 *In vitro* cellular cytotoxicity of (a) control (POM free) nanoparticles, 1%Py@NPs, 3.5%Py@NPs and 5%Py@NPs; and (b) POM-polymer hybrid nanoparticles, 1%POM@NPs, 3.5%POM@NPs and 5% POM@NPs. Error bars represent the standard deviation of the mean, calculated from three independent replicates ($n = 3$).

cytotoxicity at particle concentration above 0.1×10^9 particles per mL, with an IC_{50} value of about 0.04×10^9 particles per mL (Fig. 6b). Considering that the TOA salts of POM are insoluble in PBS, $Ba_3[B^{III}W_{11}O_{39}Co^{III}(H_2O)]$, the barium salts of POM, were employed as an additional control group. Interestingly, the POM solution showed low toxicity with different cell lines, including HEK cells, human dermal fibroblast (HDF) cells (ATCC PCS-201-010) and J774.1A macrophages (ATCC TIB-67), with over 80% viability, up to a concentration of 500 μM (Fig. S24–S26†). In comparison, the highest POM concentration used in the nanoparticle cell viability tests was over an order of magnitude lower *ca.* 40 μM (5%POM@NPs, 50×10^9 particles per mL). Based on our observations, it can be concluded that the polymeric matrix, as well as the polyanion cross-linkers, have promising biocompatibilities with HEK cells, and the enhanced cytotoxicity at low particle concentrations ($<0.5 \times 10^9$ particles per mL) might be attributable to the effective release of TOA. This is the subject of further investigation with a modified synthetic procedure for POM-polymer hybrid materials under exploration.

Conclusions

We have developed a series of novel POM-polymer coordination materials with pH/redox dual-responsiveness. By integrating charge-shifting and redox-responsive functionalities within a single system, these hybrid nanoparticles experienced a two-stage structural transform in response to acidification and mild reducing conditions, while maintaining superior colloidal stability under extracellular conditions. During the first pH-responsive stage, the controlled release of TOA, the charge-balancing cation of POMs, was observed under endosomal pH conditions. This was followed by rapid particle destabilisation in the second redox-responsive stage, triggered by the addition of 5 mM DTT. These observations suggested that POMs functioned as redox-sensitive cross-linkers within this pH-responsive system. Specifically, they prevented the particles disassembly at pH level below the pK_a of charge-shifting polymers by enhancing hydrogen bonding and charge interactions between the polymers and polyanions. The reduction of cobalt(III) and the subsequent cleavage of coordination bond following treatment with reducing agents led to the disintegration of the hybrid assemblies. As an initial proof of concept, this work focuses on the development and characterization of these stimuli-responsive hybrid nanoparticles, establishing a platform for future drug delivery applications. Essential next steps will include cation replacement (such as substituting the toxic TOA) and therapeutic encapsulation and release *via* hydrophobic interactions or cleavable linkages to fully explore the application potential of this platform. In conclusion, the facile construction of pH- and redox-responsive nanoparticles represented a novel approach for developing more efficient intracellular drug delivery systems.

Data availability

All experimental data, and detailed experimental procedures are available in the ESI.†

Author contributions

Conceptualisation, Y. G., G. K. S., C. R.; investigation, methodology and data acquisition and curation, Y. G.; data acquisition, F. Y., Y. W., R. N. D.; writing – original draft preparation, Y. G; writing – review and editing, all authors; funding acquisition, G. K. S., C. R. All authors have approved the final version of the manuscript and the ESI.†

Conflicts of interest

There are no conflicts to declare.

Acknowledgements

C. R. would like to thank Monash University and the Australian Research Council for funding this research (FT180100610). G. S Would like to the thank the Australian Research Council for funding this research (DP240102642). Y. G. would like to acknowledge the support of the University of Melbourne through the Melbourne Research Scholarship and the Dr Albert Shimmins Fund. We would like to acknowledge the Bio21 Lan Holmes Imaging Centre for support with Cryo-EM.

References

1 K. Cho, X. Wang, S. Nie, Z. Chen and D. M. Shin, *Clin. Cancer Res.*, 2008, **14**, 1310–1316.
2 P. Couvreur, *Adv. Drug Deliv. Rev.*, 2013, **65**, 21–23.
3 M. J. Mitchell, M. M. Billingsley, R. M. Haley, M. E. Wechsler, N. A. Peppas and R. Langer, *Nat. Rev. Drug Discov.*, 2021, **20**, 101–124.
4 K. L. Herpoldt, C. L. López, I. Sappington, M. N. Pham, S. Srinivasan, J. Netland, K. S. Montgomery, D. Roy, A. N. Prossnitz and D. Ellis, *Adv. Healthcare Mater.*, 2024, 2303910.
5 M. A. Beach, U. Nayanathara, Y. Gao, C. Zhang, Y. Xiong, Y. Wang and G. K. Such, *Chem. Rev.*, 2024, **124**, 5505–5616.
6 H.-C. Huang, S. Barua, G. Sharma, S. K. Dey and K. Rege, *J. Contr. Release*, 2011, **155**, 344–357.
7 B. S. Pattni, V. V. Chupin and V. P. Torchilin, *Chem. Rev.*, 2015, **115**, 10938–10966.
8 K. Song, D. C. Nguyen, T. Luu, O. Yazdani, D. Roy, P. S. Stayton and S. H. Pun, *J. Controlled Release*, 2023, **356**, 232–241.
9 S. Mura, J. Nicolas and P. Couvreur, *Nat. Mater.*, 2013, **12**, 991–1003.
10 A. Raza, T. Rasheed, F. Nabeel, U. Hayat, M. Bilal and H. M. Iqbal, *Molecules*, 2019, **24**, 1117.
11 C. M. Wells, M. Harris, L. Choi, V. P. Murali, F. D. Guerra and J. A. Jennings, *J. Funct. Biomater.*, 2019, **10**, 34.
12 C. Li, Z. Deng and E. R. Gillies, *Curr. Opin. Biomed. Eng.*, 2023, **25**, 100437.
13 Q. E. Sirianni, T. Wang, A. Borecki, Z. Deng, J. A. Ronald and E. R. Gillies, *Biomater. Sci.*, 2022, **10**, 2557–2567.
14 G. K. Such, Y. Yan, A. P. Johnston, S. T. Gunawan and F. Caruso, *Adv. Mater.*, 2015, **27**, 2278–2297.
15 M. C. Arno, J. D. Simpson, L. D. Blackman, R. P. Brannigan, K. J. Thurecht and A. P. Dove, *Biomater. Sci.*, 2023, **11**, 908–915.
16 A. Balaji, A. R. Prior, R. K. O'Reilly, A. P. Dove, K. J. Thurecht and C. A. Bell, *Polym. Chem.*, 2024, **15**, 1152–1165.
17 G. J. Doherty and H. T. McMahon, *Annu. Rev. Biochem.*, 2009, **78**, 857–902.
18 X. Du, L. Xiong, S. Dai and S. Z. Qiao, *Adv. Healthcare Mater.*, 2015, **4**, 771–781.
19 N. Deirram, C. Zhang, S. S. Kermaniyan, A. P. Johnston and G. K. Such, *Macromol. Rapid Commun.*, 2019, **40**, 1800917.
20 J. T. Wilson, A. Postma, S. Keller, A. J. Convertine, G. Moad, E. Rizzardo, L. Meagher, J. Chiefari and P. S. Stayton, *AAPS J.*, 2015, **17**, 358–369.
21 N. Kongkatigumjorn, S. A. Smith, M. Chen, K. Fang, S. Yang, E. R. Gillies, A. P. Johnston and G. K. Such, *ACS Appl. Nano Mater.*, 2018, **1**, 3164–3173.
22 A. S. Wong, E. Czuba, M. Z. Chen, D. Yuen, K. I. Cupic, S. Yang, R. Y. Hodgetts, L. I. Selby, A. P. Johnston and G. K. Such, *ACS Macro Lett.*, 2017, **6**, 315–320.
23 M. A. Beach, S. L. Teo, M. Z. Chen, S. A. Smith, C. W. Pouton, A. P. Johnston and G. K. Such, *ACS Appl. Mater. Interfaces*, 2021, **14**, 3653–3661.
24 J. Dai, S. Lin, D. Cheng, S. Zou and X. Shuai, *Angew. Chem.*, 2011, **40**, 9576–9580.
25 U. Nayanathara, B. Rossi Herling, N. Ansari, C. Zhang, S. R. Logan, M. A. Beach, S. A. Smith, N. R. Boase, A. P. Johnston and G. K. Such, *ACS Appl. Nano Mater.*, 2023, **6**, 10015–10022.
26 H. Yang, Q. Wang, S. Huang, A. Xiao, F. Li, L. Gan and X. Yang, *ACS Appl. Mater. Interfaces*, 2016, **8**, 7729–7738.
27 W. Chen, F. Meng, R. Cheng, C. Deng, J. Feijen and Z. Zhong, *J. Contr. Release*, 2015, **210**, 125–133.
28 J. Zhao, C. Yan, Z. Chen, J. Liu, H. Song, W. Wang, J. Liu, N. Yang, Y. Zhao and L. Chen, *J. Colloid Interface Sci.*, 2019, **540**, 66–77.
29 Z. Zhao, H. Fan, G. Zhou, H. Bai, H. Liang, R. Wang, X. Zhang and W. Tan, *J. Am. Chem. Soc.*, 2014, **136**, 11220–11223.
30 W. Zhou, T. Pan, H. Cui, Z. Zhao, P. K. Chu and X. F. Yu, *Angew. Chem.*, 2019, **131**, 779–784.
31 Y. Gao, M. Choudhari, G. K. Such and C. Ritchie, *Chem. Sci.*, 2022, **13**, 2510–2527.
32 A. Elliott, J. McAllister, D. L. Long, Y. F. Song and H. N. Miras, *Angew. Chem.*, 2023, **135**, e202218897.
33 I. Colliard, J. R. Lee, C. A. Colla, H. E. Mason, A. M. Sawvel, M. Zavarin, M. Nyman and G. J.-P. Deblonde, *Nat. Chem.*, 2022, **14**, 1357–1366.
34 D. E. Salazar Marcano, S. Lentink, J. J. Chen, A. V. Anyushin, M. A. Moussawi, J. Bustos, B. Van Meerbeek, M. Nyman and T. N. Parac-Vogt, *Small*, 2024, 2312009.
35 A. Barba-Bon, N. I. Gumerova, E. Tanuhadi, M. Ashjari, Y. Chen, A. Rompel and W. M. Nau, *Adv. Mater.*, 2024, **36**, 2309219.
36 G. Guedes, S. Wang, H. A. Santos and F. L. Sousa, *Eur. J. Inorg. Chem.*, 2020, **2020**, 2121–2132.
37 X. Kong, G. Wan, B. Li and L. Wu, *J. Mater. Chem. B*, 2020, **8**, 8189–8206.
38 X. Wang, S. Wei, C. Zhao, X. Li, J. Jin, X. Shi, Z. Su, J. Li and J. Wang, *JBIC, J. Biol. Inorg. Chem.*, 2022, **27**, 405–419.
39 C. McWilliams, I. F. Castillo, A. Seral-Ascaso, S. García-Embid, M. Malefioudaki, J. G. Meier, R. Martín-Rapún and S. G. Mitchell, *RSC Pharm.*, 2024, **1**, 755–764.
40 T. Yamase, *J. Mater. Chem.*, 2005, **15**, 4773–4782.
41 A. Ogata, H. Yanagie, E. Ishikawa, Y. Morishita, S. Mitsui, A. Yamashita, K. Hasumi, S. Takamoto, T. Yamase and M. Eriguchi, *Br. J. Cancer*, 2008, **98**, 399–409.
42 A. Bijelic, M. Aureliano and A. Rompel, *Angew. Chem., Int. Ed.*, 2019, **58**, 2980–2999.
43 Y. Gao, J. Xu, C. Zhang, H. Venugopal, S. S. Kermaniyan, G. Such and C. Ritchie, *ACS Appl. Nano Mater.*, 2020, **3**, 11247–11253.
44 J. Xu, H. Volfova, R. J. Mulder, L. Goerigk, G. Bryant, E. Riedle and C. Ritchie, *J. Am. Chem. Soc.*, 2018, **140**, 10482–10487.
45 D. Xiao, H.-Z. Jia, N. Ma, R.-X. Zhuo and X.-Z. Zhang, *Nanoscale*, 2015, **7**, 10071–10077.
46 K. Nakamura, K. Nakabayashi, K. Imoto and S.-i. Ohkoshi, *Inorg. Chem. Front.*, 2023, **10**, 850–859.
47 C. L. Cooper, T. Cosgrove, J. S. van Duijneveldt, M. Murray and S. W. Prescott, *Soft Matter*, 2013, **9**, 7211–7228.